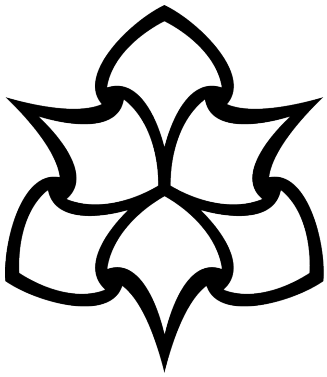

A coupled overset CFD and mooring line model for floating wind turbine hydrodynamics

Zaibin Lin, Ling Qian and Wei Bai
Centre for Mathematical Modelling and Flow Analysis, Department of Computing and Mathematics,
Manchester Metropolitan University, Manchester, M1 5GD, United Kingdom

ABSTRACT

To capture wind energy in the windiest parts of the ocean, floating wind turbines, which are designed to work in deep waters, have to be deployed. To support the wind turbines, floaters, such as spar-buoy, semi-submersible, and tension leg platforms, are commonly adopted, which are tethered to the seabed via mooring lines in order to restrain their motions. In this work, to evaluate dynamic response of floating offshore wind turbines (FOWTs) under the action of waves, an overset mesh based multi-phase flow solver is applied to model the wave structure interaction problem due to its proven capability to accurately capture large amplitude motions of structures. In the meantime, the quasi-static mooring line model is integrated into the overset mesh CFD model so the effects of both waves and mooring systems on FOWTs can be simulated. To validate the coupled model, a test case that involves a moored semi-submersible floating wind turbine model under the action of waves only is simulated and the predicted heave and pitch motions are compared with available experimental data and other numerical work. The validated overset CFD-mooring line model is then applied to investigate the dynamic motion response of the semi-submersible floater in waves of various steepness and periods including focused wave groups, demonstrating its accuracy and capability for FOWT applications.

KEY WORDS: OpenFOAM; Finite volume method; Overset mesh solver; Quasi-Static mooring system.

INTRODUCTION

Continuously growing demand of clean energy from the ocean has driven a rapid development of both offshore renewable energy industry and research. One of the mostly popular technologies of utilising offshore renewable energy is to install the wind turbines on either fixed or floating structures in the ocean. For the floating structures in the deep sea, there are several types of platforms that have already been widely used in offshore oil and gas industry, such as semi-submersible, tension-leg, and spar platforms. Although the technology to be adopted for floating offshore wind turbines (FOWTs) is similar to that used in oil and gas industry, there are important differences in the mass (size) and wave/wind loading characteristics between the two structures, hence the need for a specific evaluation of the hydrodynamic characteristics especially their stability and survivability under extreme conditions. To address these issues, a high-fidelity numerical model needs to be developed to accurately and simultaneously model hydrodynamics and aerodynamics of floaters and turbine rotors respectively, as well as mooring loads.

As one of the most well-known codes for modelling floating offshore wind turbine systems, the FAST (Fatigue, Aerodynamics, Structures, and Turbulence), which was implemented by the National Renewable Energy Laboratory (NREL), has proven to be a powerful tool. For the prediction of hydrodynamics, the FAST relies on the results from external potential flow theory based hydrodynamic models as the inputs, such as WAMIT and AQWA (Yang et al., 2020). Due to the assumption of potential flow theory, these hydrodynamic models are not able to accurately capture the motion response of a floating platform in extreme environmental conditions, which in turn will potentially affect the prediction accuracy of the other model components in the FAST. Thus, to better predict the hydrodynamic response and survivability of a floating offshore wind turbine, a numerical model that takes the full non-linearity of the free surface problems into account, including wave breaking process, is needed.

Compared to the numerical models based on fully nonlinear potential flow theory e.g. Yan and Ma (2007) and Q Ma and Yan (2009), the numerical models based on Navier-Stokes equations and Volume of Fluid (NS-VoF) are able to predict the flow details in the vicinity of a floating platform and corresponding motion response under extreme ocean conditions (Chen et al., 2020; Lin et al., 2020). In order to investigate the dynamics of a spar buoy floating wind turbine in waves, Nematbakhsh et al. (2013) developed a 3-Dimensional (3D) numerical wave tank based on Navier-Stokes equations, where the air-water interface was tracked by Level Set Method and the immersed boundary method was implemented at the solid surface of the support structure. Zhao and Wan (2015) adopted the naoe-FOAM-SJTU solver in OpenFOAM to investigate the wave-induced motion response of an OC4 (Offshore Code Comparison Collaboration Continuation project) semi-submersible floater in waves, taking into account the effects

of wind-induced force and moments acting on the floater rotational centre. By using the STAR-CCM+ software, Tran and Kim (2015) investigated the dynamic response of a semi-submersible floater with catenary mooring lines in waves. It was concluded that their coupled model has the capability of accurately reproducing experimental results without the use of tuning parameters, which was the common approach in potential flow theory based models. Subsequently Tran and Kim (2016) performed the numerical investigations of the fully coupled aero-hydrodynamics analysis of a semi-submersible floating offshore wind turbine by applying the overset mesh technique in STAR-CCM+. Good agreements have been demonstrated by comparing the numerical results from their proposed models, experimental measurements, and the simulation results based on the FAST. By using the sliding mesh technique in OpenFOAM, Liu et al. (2017) implemented a fully coupled CFD model for floating offshore wind turbines, taking both aerodynamics and hydrodynamics into consideration.

More recently, Bruinsma et al. (2018) presented an improved Navier-Stokes/Six Degree of Freedom (6-DoF) motion solver in OpenFOAM for FOWT applications, and performed extensive validations against experimental measurements from the OC5 programme. It is worth noting that this work was among the first to provide a detailed comparison of the time histories of FOWT platform motion responses between the numerical predictions and the experiments. Subsequently, Rivera-Arreba et al. (2018) compared the numerical results from a second-order potential flow model and the NS-VoF model with the experimental data in terms of heave and pitch response in non-steep waves. For more extreme cases, it was found that when the floater is excited at the heave natural frequency the potential flow based model failed to predict the heave response accurately due to its inherent limitations.

To better capture the dynamic response of FOWT floaters under extreme waves and to avoid mesh distortion induced by large amplitude 6-DoF platform motions, in the present work an overset mesh based multi-phase flow solver in OpenFOAM (Chen et al., 2019) is integrated with the Quasi-Static mooring line model as implemented in Bruinsma et al. (2018). This newly proposed model is first validated against relevant experimental data and numerical results based on dynamic mesh solver (interDyMFoam/waveDyMFoam) for a test case involving a moored semi-submersible FOWT floater in regular waves. Then, the validated model is further applied to study the motion response of the semi-submersible floater in regular waves and focused wave groups of various wave heights and periods to demonstrate its ability to predict dynamic response of FOWTs under different conditions. Finally, in the last section the conclusions based on the model validations and applications are briefly summarised.

NUMERICAL MODELS

Governing equations

The two phase flow problem is governed by incompressible Navier-Stokes equations and the air-water interface is captured by the Volume of Fluid method.

$$\nabla \cdot \boldsymbol{u} = 0 \tag{1}$$

$$\frac{\partial \rho \boldsymbol{u}}{\partial t} + \nabla \cdot (\rho \boldsymbol{u})\boldsymbol{u} - \nabla \cdot \mu \nabla \boldsymbol{u} = -\nabla p^* - (\boldsymbol{g} \cdot \boldsymbol{x})\nabla \rho \tag{2}$$

$$\frac{\partial \alpha}{\partial t} + \nabla \cdot \boldsymbol{u}\alpha + \nabla \cdot (\boldsymbol{u}_r \alpha(1-\alpha)) = 0 \tag{3}$$

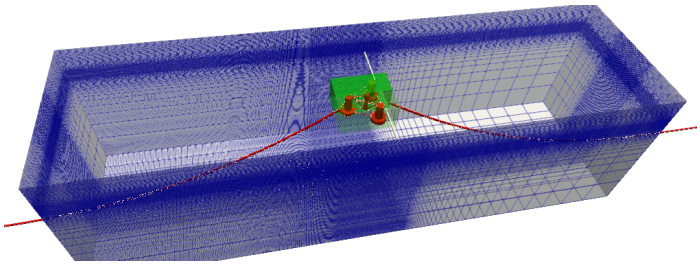

(a) Overall mesh setup of numerical wave tank and green zone is the overset mesh region.

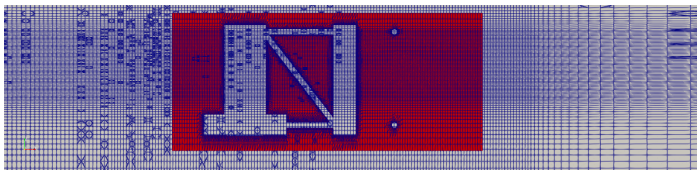

(b) Mesh setups of overset mesh (red zone) and background mesh in the vicinity of a semi-submersible floater.

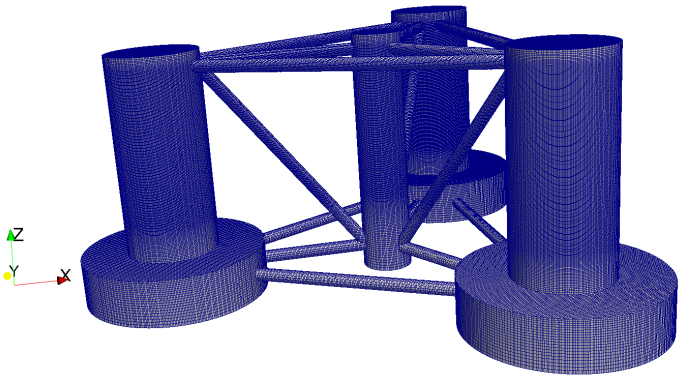

(c) Surface mesh of a semi-submersible floater.

Fig. 1 Mesh setups for numerical wave tank.

where ρ is fluid density, t is time, $\boldsymbol{u}$ is the velocity field, μ is dynamic viscosity of fluid, p^* is the pressure in excess of static pressure, $\boldsymbol{g}$ is gravitational acceleration, $\boldsymbol{x} = (x, y, z)$ is the Cartesian coordinate system, α is the volume fraction, and $\boldsymbol{u_r}$ is compressive velocity field (Berberović et al., 2009) for maintaining the sharp water-air interface. All these equations are spatially discretised and solved by Finite Volume Method in the open source Computational Fluid Dynamics toolbox OpenFOAM.

Overset mesh solver and mooring line model

To avoid potential mesh distortion due to the large motion of a moving structure, the overset mesh functionality implemented in OpenFOAM was adopted in this study for modelling a semi-submersible FOWT floater in both regular and focused waves. In general, overset mesh technique is clearly advantageous over the dynamic (moving) mesh approach as far as modelling flow problems with large amplitude uniform or relative body motions is concerned. The basic concept of overset mesh technique is quite simple - there are multiple meshes (grids) in a composite mesh system, i.e., one background mesh covering the entire computational domain and one or more overset meshes on top of it. During the simulation, the background mesh is fixed and an overset mesh is generated around each structure and moves with it. The flow variables between the background and overset meshes are exchanged by interpolation at each time step. More details of the implementation of overset mesh technique in OpenFOAM can be found in Chen et al.

(2019) and Z Ma et al. (2018).

As semi-submersible floaters are installed in deep waters, their motions are restrained by catenary type mooring lines, which are anchored into seabed. In this work, to model the mooring line dynamics a Quasi-Static (Q-S) mooring line model is adopted and integrated into the overset multi-phase flow solver in OpenFOAM. The effectiveness and accuracy of the mooring line model has previously been demonstrated in Bruinsma et al. (2018) and for the details of the model, readers are referred to Krenk (2001) and Bruinsma et al. (2018).

MODEL VALIDATION

To validate the coupled overset mesh and mooring line solver in OpenFOAM, a test case involving a 1:50 scale semi-submersible FOWT model under the action of regular waves is simulated. The physical experiments were conducted at the MARIN, the Netherlands. In the experiments, two catenary mooring lines and two linear springs were installed to the floater to restrain its motion response. For more details on the mooring lines setup, such as mooring attachment and anchor locations, and mooring lines properties, readers are referred to the Appendix D in Bruinsma (2016). The wave parameters used for the validation test case are listed as case RWA1 in Table 2 and the structural properties of the semi-submersible floater are listed in Table 1, where the full mass properties of the FOWT model are considered, including nacelle, rotor blades, support tower, semi-submersible floater and mooring lines. The numerical wave tank has a length of 18m, width of 5m, and height of 5m. The skech of numerical wave tank is illustrated in Fig. 1(a), where the inlet for wave generation is applied on left boundary, outlet for absorbing outgoing waves is imposed on right end boundary, the atmosphere boundary condition is used on the top of NWT, and the side and bottom are treated as wall boundary condition. The mesh cell numbers of the background and overset meshes are 3.4 million and 1.75 million, respectively. For the background mesh a minimum of 80 cells per wave length are used in the direction of wave propagation and the region around the floater in Fig.1(b), where the floating structure may move under the effects of waves, is refined adequately to capture the details of the wave-structure interaction process. The applied mesh resolution is based on our previous mesh convergence studies in Lin et al. (2020) for simulating the interaction between focused waves and wave energy converters. To represent the floater in the overset mesh zone accurately, a well refined surface mesh has been used as indicated in Fig.1(c). During the simulation, each time step is determined by Courant–Friedrichs–Lewy condition, which is 0.3 in all the cases followed. Finally, in the numerical wave tank, the target or required waves are generated and absorbed at the two ends of the numerical wave tank using IHFOAM package (Higuera et al., 2013a,b).

In Fig. 2, the numerical results based on the present overset-mooring line model are compared with the experimental measurements and numerical results based on the dynamic mesh solver with the same Q-S mooring model in OpenFOAM. It can be seen that while no experimental and other numerical results of the surge motion are available for comparison, the numerical results from the present overset-mooring model have better agreements with the experimental measurements for both heave and pitch responses. This shows that compared with the dynamic mesh solver in OpenFOAM, the overset mesh solver can achieve better solution accuracy when a structure of complex geometry such as the semi-submersible floater and its motion response due to waves are considered. For the computational expense, this validation case took approximately 137.2 hours using 96 cores with Intel® Xeon® E5 2603 @ 1.7GHz.

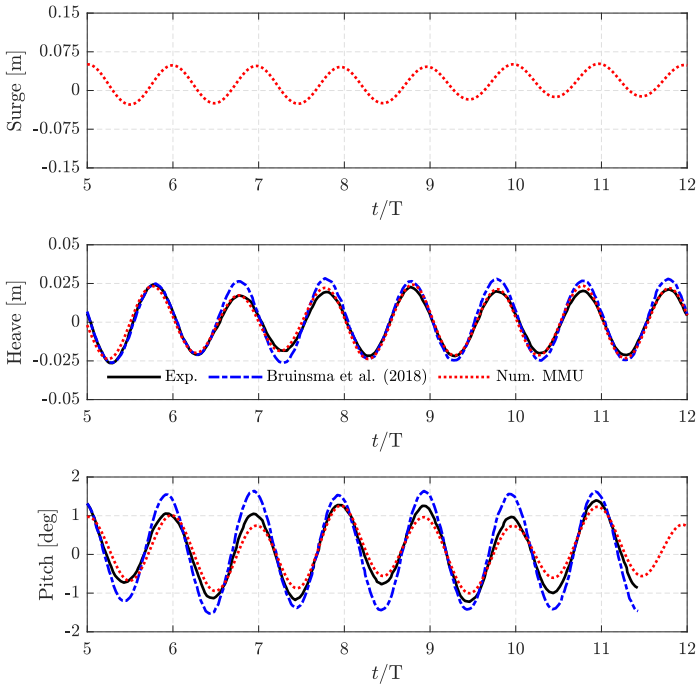

Fig. 2 Validations of motion response under regular waves (RWA1 in Table 2) against experimental measurements and numerical results from Bruinsma et al. (2018).

Table 1 Mass properties of the semi-submersible floater.

M [kg]	I_{xx} [kgm^2]	I_{yy} [kgm^2]	I_{zz} [kgm^2]	d [m]	CoM [m]
111.66	49.77	47.56	43.81	0.4	0.1614

Note: M is the mass of a semi-submersible floater; I_{xx}, I_{yy}, and I_{zz} are the moment of inertia; d is the draft, and CoM is the centre of mass below still water level. The mass properties take full floating system into consideration, including a nacelle, rotor blades, a support tower, a floater, and mooring lines.

Table 2 Wave parameters of regular waves with various wave amplitudes and same wave period

Case ID	Wave amplitude (m)	Wave period (s)	Water depth (m)
RWA1	0.07	1.71	4
RWA2	0.09	1.71	4
RWA3	0.13	1.71	4
RWA4	0.17	1.71	4

APPLICATIONS AND DISCUSSIONS

In this section, the developed overset-mooring line model is further applied to investigate motion response of the aforementioned floater in regular waves with various wave amplitudes and wave periods (constant wave steepness) and focused waves with various peak wave amplitudes.

Table 3 Wave parameters of regular waves with various wave periods and constant wave steepness

Case ID	Wave amplitude (m)	Wave period (s)	Water depth (m)	Wave steepness (ka)
RWT1	0.13	1.71	4	0.179
RWT2	0.18	2	4	0.179
RWT3	0.234	2.3	4	0.179
RWT4	0.296	2.6	4	0.179
RWT5	0.36	2.9	4	0.179

Motion response under regular waves

A preliminary parametric study on the effects of wave amplitudes (steepness) and wave periods (with constant wave steepness) on motion response of the semi-submersible floater under regular waves are conducted. Four test cases for the former and five test cases for the latter have been chosen and the corresponding wave parameters are tabulated in Tables 2 and 3.

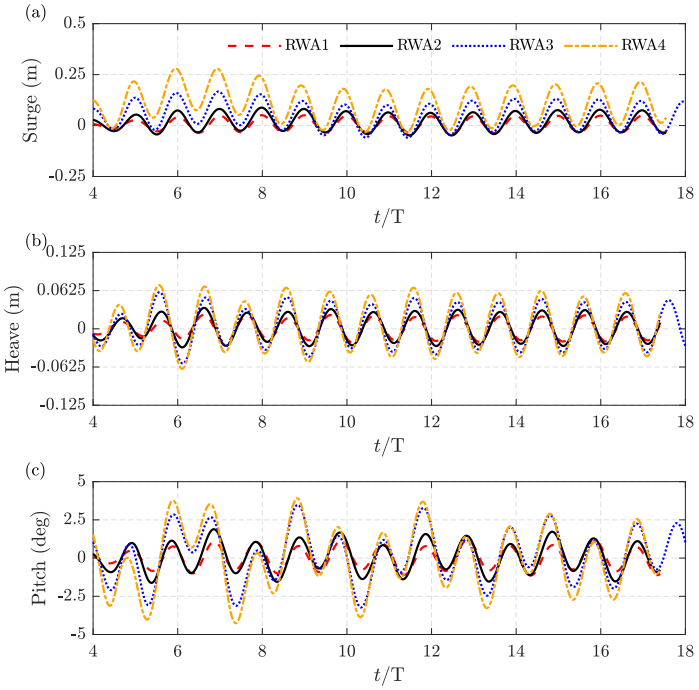

Fig. 3 Motion response of a semi-submersible floater in regular waves with various wave amplitudes in Table 2. (a) Surge; (b) Heave; (c) Pitch.

In Fig. 3, the time series of surge, heave, and pitch responses are presented with various wave amplitudes. With the increase of wave amplitudes, the magnitude of these three degree of freedoms are significantly affected and amplified. Moreover, distinct wave drift (surge) motion, which is defined the averaged surge motion away from initial location (surge = 0 m), is predicted for the case RWA4 in Fig. 3 compared to the surge for the case RWA1. On the other hand, this wave drift motion is not significant for the cases of the fixed wave steepness in Fig. 4, although the magnitude of surge for case RWT5 is still large compared to that of case RWT1. For heave motion, increasing wave amplitudes and wave periods have certainly resulted in larger heave response, particularly for the cases of larger wave periods and associated

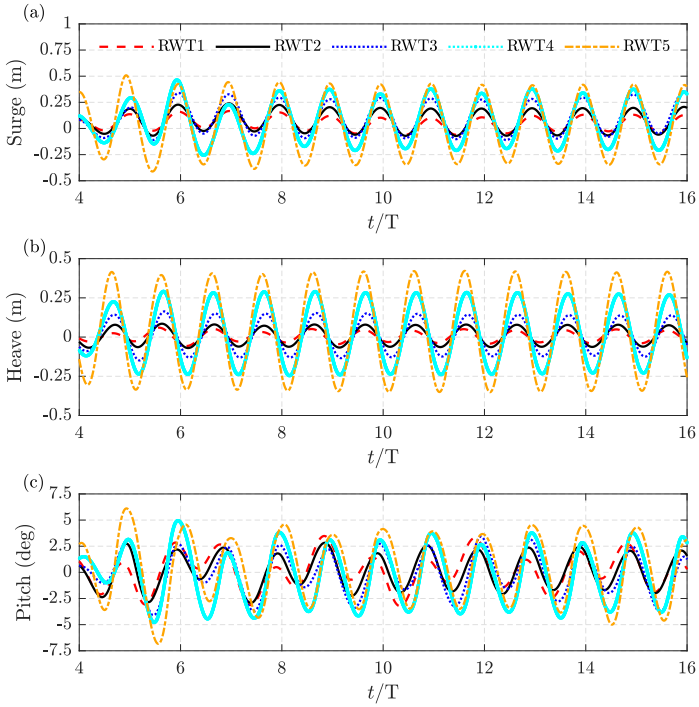

Fig. 4 Motion response of a semi-submersible floater in regular waves with various wave periods and constant wave steepness in Table 3. (a) Surge; (b) Heave; (c) Pitch.

Table 4 Test conditions of the focused wave groups

Case ID	A_f [m]	T_p [s]	H_s [m]	h [m]	k_pA [-]
FW1	0.2	2.5	0.274	4	0.128778
FW2	0.25	2.5	0.274	4	0.160972
FW3	0.3	2.5	0.274	4	0.193167

Note: A_f is focal crest height, T_p is the wave period for the wave component at peak frequency. H_s is significant wave height, h is water depth, and k_pA is wave number for the wave component at the peak frequency. Pierson-Moskowitz spectrum is adopted in this study.

higher wave amplitudes with constant wave steepness. For pitch motion, it should be noted in Fig. 3(c) that increasing wave amplitudes lead to severe rotational response compared to small wave amplitude cases. This may be attributed to the combined effects of larger wave runup and pressure difference on front and rear columns and pontoons of the floater, as well as the resulting larger overturning moments particularly at some time instants, such as t/T = 6.8, 7.34 and 8.89 in Fig. 3(c) and Fig. 5. However, the pitch response is less sensitive to the the increase of wave amplitudes as shown in cases RWA3 and RWA4. This may be due to the stronger restraints of the catenary mooring lines on the floater in the cases of large wave amplitudes.

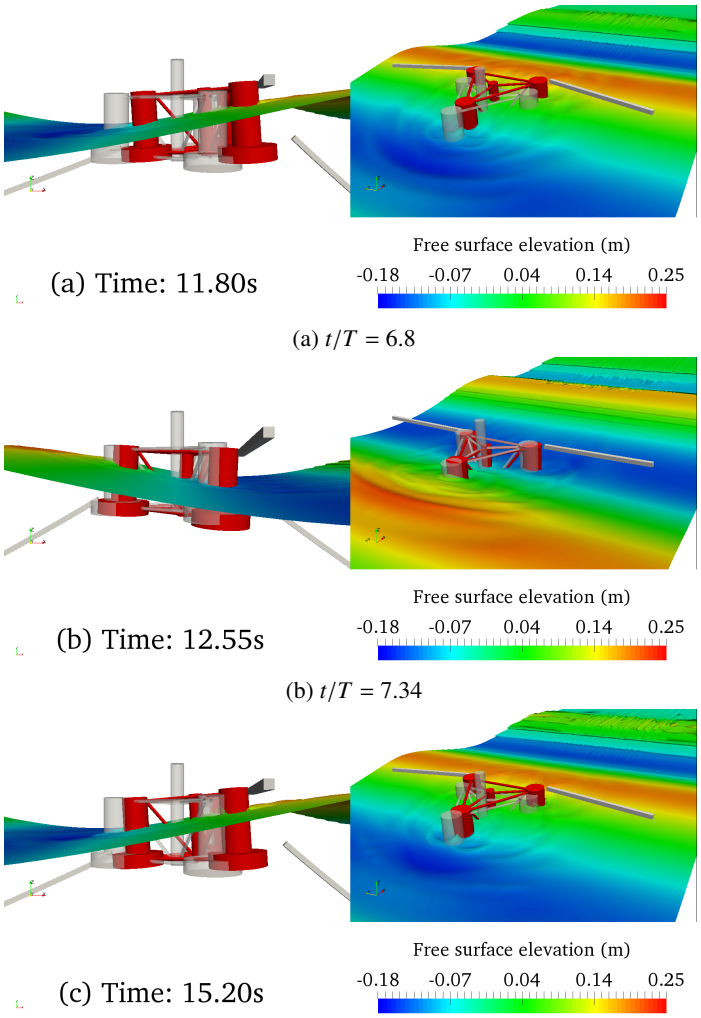

Fig. 5 Snapshots of floater motions at different time instants.

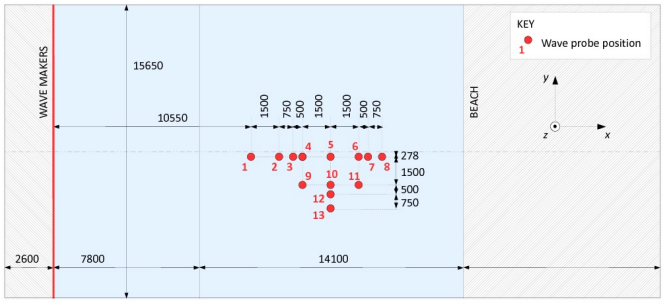

Fig. 6 The layout of wave gauges in the COAST Laboratory Ocean Basin, University of Plymouth, the UK. Source: CCP-WSI Blind Test Series 2 (2020)

Motion response under focused waves

In this section, the dynamic motion response of the semi-submersible floater in focused waves is numerically investigated. The focused waves as specified in the CCP-WSI blind test series 2 and 3 in Ransley et al. (2020) and Ransley et al. (2020) are first numerically reproduced in the empty NWT, which has a length of 24m, width of 5m, and height of 5m. The cell numbers for the background and overset meshes are 8.36 million and 1.75 million, respectively. The mesh setup of overset mesh in the vicinity of the floater is identical to the mesh setup for regular waves in Fig. 1(b) and (c). Moreover, the mooring line systems used in the regular wave tests are also adopted for the cases of focused waves. The locations of wave probes are indicated in Fig. 6. For more details of experimental setups, readers are referred to the CCP-WSI blind test series in Ransley et al. (2020), Ransley et al. (2020), Chen et al. (2020), and Lin et al. (2020). The test conditions are listed in Table 4, where the NewWave type focused wave groups are used to produce extreme wave conditions and the Pierson-Moskowitz spectrum is adopted in this study.

In Figs. 7-9, the numerical results of the focused wave groups generated by the second-order irregular wave theory (Hu et al.,2016; Chen et al., 2019) are compared with experimental data from CCP-WSI blind test series. It can be seen from the comparisons in Figs. 7-9 that excellent agreements between numerical and experimental results have been achieved. Then the test cases of the semi-submersible floater in focused waves of different peak wave amplitudes are simulated. The numerical results of motion responses, such as surge, heave, and pitch, are presented in Fig. 10, where the changes (increases) in surge and heave responses are strongly correlated to the changes (increases) of peak wave amplitudes. However, for the pitch responses the trend is slightly different. Similar to the cases of regular waves in Fig. 3(c), with the further increase of peak wave amplitudes, the change in pitch responses is somehow limited as the effects of catenary moorings on limiting the overturning motion of the floater become dominant in the conditions of larger wave amplitudes.

CONCLUSIONS AND DISCUSSION

In this study, the overset mesh solver is coupled with Q-S mooring system in OpenFOAM. This developed overset-mooring model is validated against available experimental measurements and numerical results based on dynamic mesh solver in OpenFOAM and good agreements have been achieved in terms of motion response of a semi-submersible floater in regular waves. The validated model is then applied to study the motion responses of the same floater in regular waves with different wave amplitudes and a fixed period, regular waves with different wave periods and a fixed wave steepness, and focused waves with various peak wave amplitudes. It is found that the motion response of the floater is highly sensitive to both wave amplitudes and wave periods, while the maximum pitch is limited to 5° in all cases and less sensitive to the increase of wave periods due to the restraint of catenary mooring lines. The same conclusion can be made for the motion response of the floater in focused waves. In the future, the developed overset CFD-mooring line model will be extended to include the simulation of air flow around FOWT rotors so the dynamic response of an entire FOWT system under both wind and wave loading and mooring line constraints can be evaluated.

ACKNOWLEDGMENTS

This work was partially funded by the Engineering and Physical Sciences Research Council (EPSRC, UK) projects: Extreme Loading on FOWT under Complex Environmental Conditions (EP/T004150/1), A CCP on Wave Structure Interaction: CCP-WSI (EP/M022382/1) and the Supergen ORE Hub Flexible Fund project: Passive Control of Wave Induced Platform Motions for Semi-submersible FOWTs.

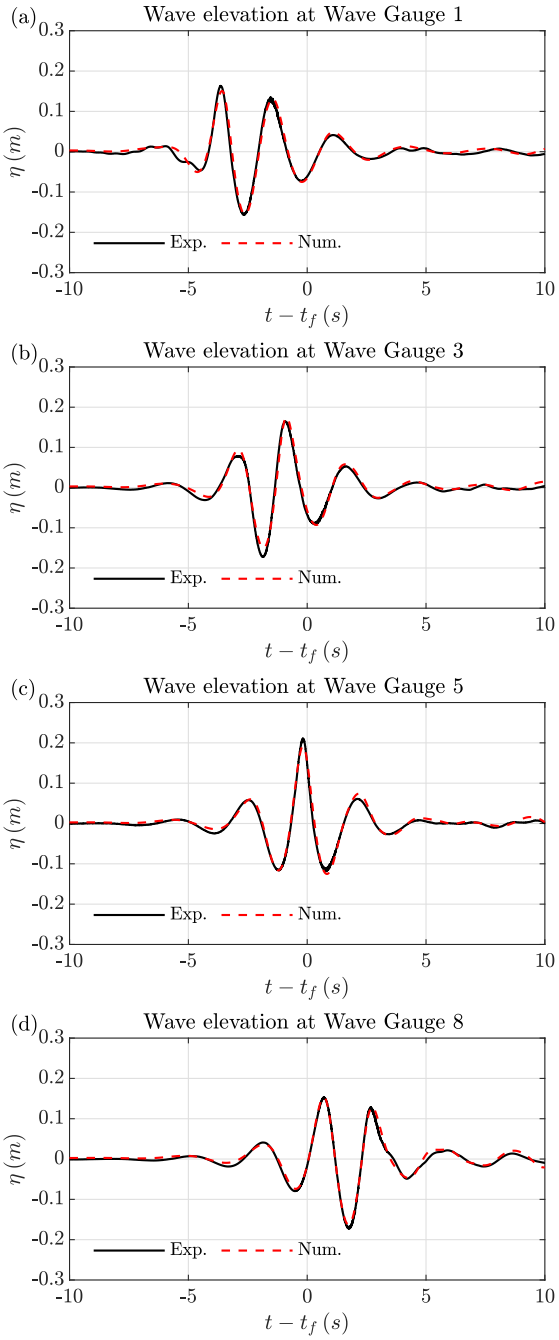

Fig. 7 Free surface elevation validation of focused waves (FW1) at different wave gauges.

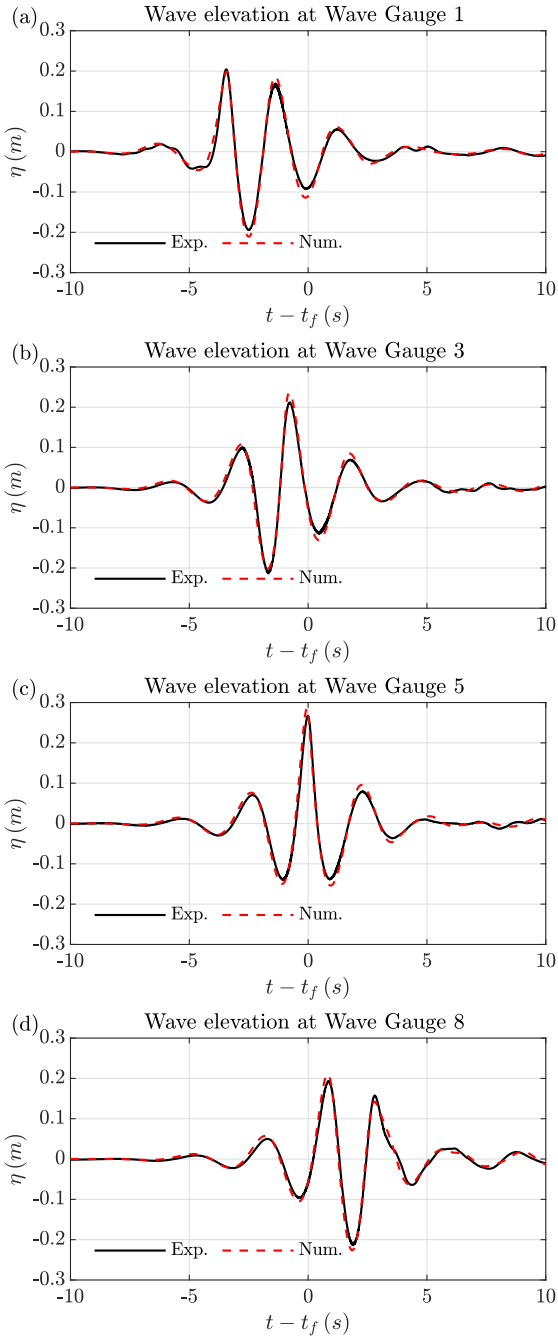

Fig. 8 Free surface elevation validation of focused waves (FW2) at different wave gauges.

REFERENCES

Berberović, E, van Hinsberg, NP, Jakirlić, S, Roisman, IV, and Tropea, C. (2009). Drop impact onto a liquid layer of finite thickness: Dynamics of the cavity evolution. *Physical Review E*, 79(3), 036306.

Bruinsma, N. (2016). Validation and application of a fully nonlinear numerical wave tank. *Delft University of Technology*, Master Thesis.

Bruinsma, N, Paulsen, B, and Jacobsen, N. (2018). Validation and application of a fully nonlinear numerical wave tank for simulating floating offshore wind turbines. *Ocean Engineering*, 147, 647–658.

CCP-WSI Blind Test Series 2. (2020). Focused wave interactions with floating structures (CCP-WSI Blind Test Series 2). [Online]. Available: https://www.ccp-wsi.ac.uk/blind_test_series_2.

Chen, H, Lin, Z, Qian, L, Ma, Z, and Bai, W. (2020). Cfd simulation of wave energy converters in focused wave groups using overset mesh. *International Journal of Offshore and Polar Engineering*, 30(01), 70–77.

Chen, H, Qian, L, Bai, W, Ma, Z, Lin, Z, and Xue, M-A. (2019). Oblique focused wave group generation and interaction with a fixed FPSO-shaped body: 3D CFD simulations and comparison with exper-

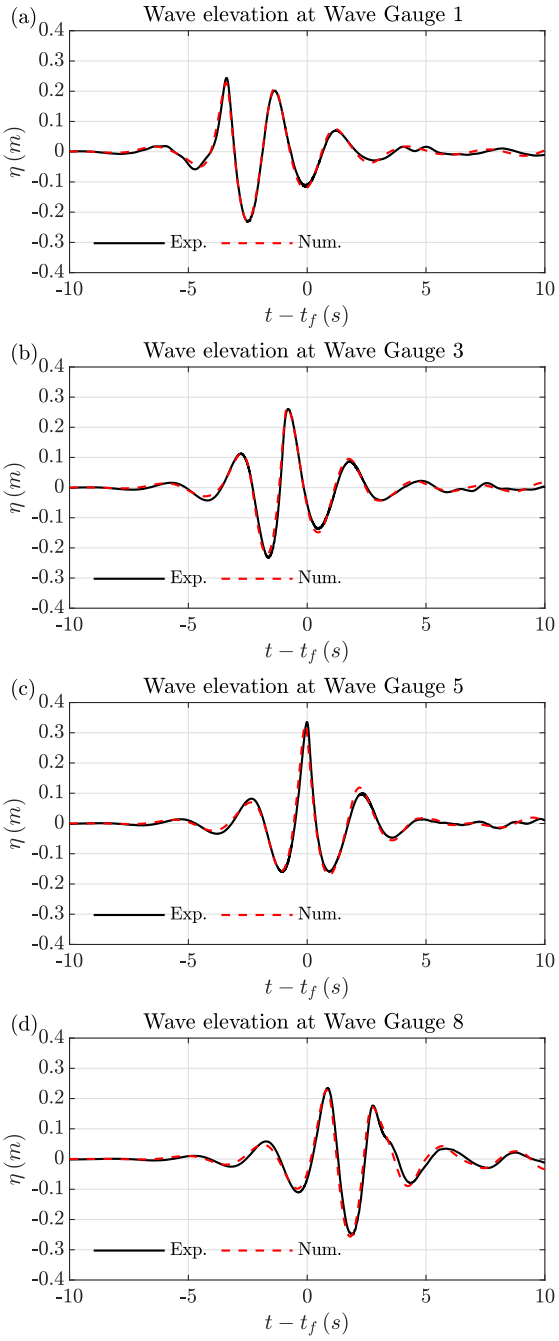

Fig. 9 Free surface elevation validation of focused waves (FW3) at different wave gauges.

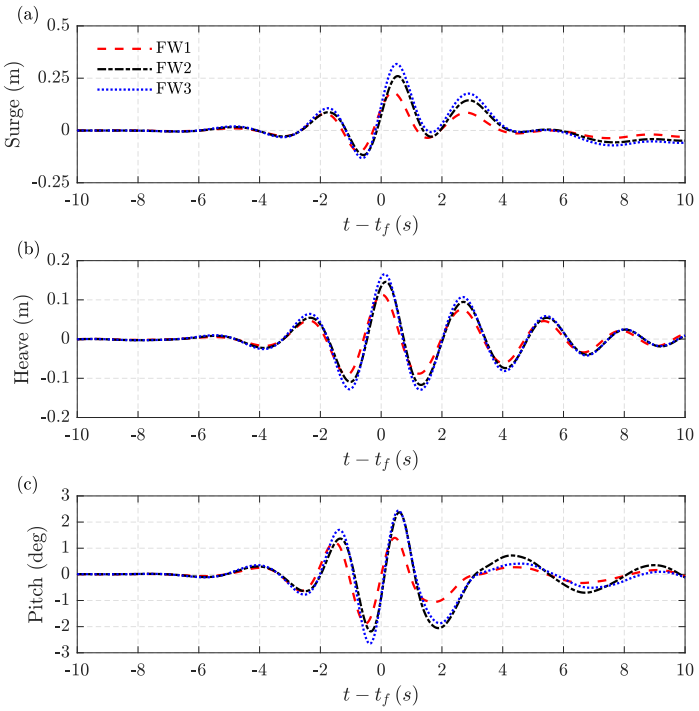

Fig. 10 Motion response of a semi-submersible floater in focused waves with various peak wave amplitude in Table 4. (a) Surge; (b) Heave; (c) Pitch.

iments. *Ocean Engineering*, 192, 106524.

Chen, H, Qian, L, Ma, Z, Bai, W, Li, Y, Causon, D, and Mingham, C. (2019). Application of an overset mesh based numerical wave tank for modelling realistic free-surface hydrodynamic problems. *Ocean Engineering*, 176, 97–117.

Higuera, P, Lara, JL, and Losada, IJ. (2013a). Realistic wave generation and active wave absorption for navier–stokes models: Application to OpenFOAM®. *Coastal Engineering*, 71, 102–118.

Higuera, P, Lara, JL, and Losada, IJ. (2013b). Simulating coastal engineering processes with OpenFOAM®. *Coastal Engineering*, 71, 119–134.

Hu, ZZ, Greaves, D, and Raby, A. (2016). Numerical wave tank study of extreme waves and wave-structure interaction using OpenFOAM®. *Ocean Engineering*, 126, 329–342.

Krenk, S. (2001). *Mechanics and analysis of beams, columns and cables: a modern introduction to the classic theories*. Springer Science & Business Media.

Lin, Z, Chen, H, Qian, L, Ma, Z, Causon, D, and Mingham, C. (2020). Simulating focused wave impacts on point absorber wave energy converters. *Proceedings of the Institution of Civil Engineers-Engineering and Computational Mechanics*, 1–34.

Liu, Y, Xiao, Q, Incecik, A, Peyrard, C, and Wan, D. (2017). Establishing a fully coupled cfd analysis tool for floating offshore wind turbines. *Renewable Energy*, 112, 280–301.

Ma, Q, and Yan, S. (2009). Qale-fem for numerical modelling of nonlinear interaction between 3d moored floating bodies and steep waves. *International Journal for Numerical Methods in Engineering*, 78(6), 713–756.

Ma, Z, Qian, L, Martinez-Ferrer, P, Causon, D, Mingham, C, and Bai, W. (2018). An overset mesh based multiphase flow solver for water entry problems. *Computers & Fluids*, 172, 689–705.

Nematbakhsh, A, Olinger, DJ, and Tryggvason, G. (2013). A nonlinear computational model of floating wind turbines. *Journal of fluids Engineering*, 135(12).

Ransley, E, Brown, S, Hann, M, Greaves, D, Windt, C, Ringwood, J, Davidson, J, Schmitt, P, Yan, S, Wang, JX, Wang, JH, Ma, Q, Xie, Z, Giorgi, G, Hughes, J, Williams, A, Masters, I, Lin, Z, Chen, H, Qian, L, Ma, Z, Chen, Q, Ding, H, Zang, J, van Rij, J, Yu, Y, Li, Z, Bouscasse, B, Ducrozet, G, and Bingham, H. (2020). Focused wave interactions with floating structures: A blind comparative study. *Proceedings*

of the Institution of Civil Engineers-Engineering and Computational Mechanics, 1–16.

Ransley, E, Yan, S, Brown, S, Hann, M, Graham, D, Windt, C, Schmitt, P, Davidson, J, Ringwood, J, Musiedlak, P-H, Wang, J, Wang, J, Ma, Q, Xie, Z, Zhang, N, Zheng, X, Giorgi, G, Chen, H, Lin, Z, Qian, L, Ma, Z, Bai, W, Chen, Q, Zang, J, Ding, H, Cheng, L, Zheng, J, Gu, H, Gong, X, Liu, Z, Zhuang, Y, Wan, D, Bingham, H, and Greaves, D. (2020). A blind comparative study of focused wave interactions with floating structures (CCP-WSI Blind Test Series 3). *International Journal of Offshore and Polar Engineering*, 30, 1-10.

Rivera-Arreba, I, Bruinsma, N, Bachynski, EE, Viré, A, Paulsen, BT, and Jacobsen, NG. (2018). Modeling of a semisubmersible floating wind platform in severe waves. In *International conference on offshore mechanics and arctic engineering* (Vol. 51302, p. V009T13A002).

Tran, TT, and Kim, D-H. (2015). The coupled dynamic response computation for a semi-submersible platform of floating offshore wind turbine. *Journal of wind engineering and industrial aerodynamics*, 147, 104–119.

Tran, TT, and Kim, D-H. (2016). Fully coupled aero-hydrodynamic analysis of a semi-submersible fowt using a dynamic fluid body interaction approach. *Renewable energy*, 92, 244–261.

Yan, S, and Ma, Q. (2007). Numerical simulation of fully nonlinear interaction between steep waves and 2d floating bodies using the qale-fem method. *Journal of Computational physics*, 221(2), 666–692.

Yang, Y, Bashir, M, Michailides, C, Li, C, and Wang, J. (2020). Development and application of an aero-hydro-servo-elastic coupling framework for analysis of floating offshore wind turbines. *Renewable Energy*, 161, 606–625.

Zhao, W, and Wan, D. (2015). Numerical study of interactions between phase ii of oc4 wind turbine and its semi-submersible floating support system. *Journal of Ocean and Wind Energy*, 2(1), 45–53.